

Article

Effects of Micro-Sized Ferrite and Austenite Grains on the Pitting Corrosion Behavior of Lean Duplex Stainless Steel 2101

Yadi Hu, Yuping Li *, Yan He, Jian Wang, Xinglong Liu, Yong Zhang and Peide Han *

Key Laboratory of Interface Science and Engineering in Advanced Materials, Ministry of Education, College of Materials Science and Engineering, Taiyuan University of Technology, Taiyuan 030024, China; 15735161312@163.com (Y.H.); heyan2012@163.com (Y.H.); wangjian@tyut.edu.cn (J.W.); 18636622604@163.com (X.L.); cclg1106@163.com (Y.Z.)

* Correspondence: yupingli123@163.com (Y.L.); hanpeide@tyut.edu.cn (P.H.); Tel.: +86-351-601-8843 (Y.L. & P.H.); Fax: +86-351-601-4208 (Y.L. & P.H.)

Academic Editor: Tiziano Bellezze

Received: 1 March 2017; Accepted: 9 May 2017; Published: 12 May 2017

Abstract: The connection between the austenite transformation and pitting corrosion of lean duplex stainless steel LDX 2101 was investigated at different annealing temperatures in the range 950–1200 °C. Optical microscopy, scanning electron microscopy, and electrochemical techniques were employed in the present work. Results indicated that micro-sized ferrite and austenite grains, formed with the increase of annealing temperature, influenced the pitting corrosion resistance of the studied stainless steel. As the austenite phase transformed into ferrite, the micro-sized ferrite grains were produced in austenite domains with temperature increase from 1000 °C to 1100 °C, especially at 1050 °C. In these conditions, the corrosion resistance of LDX 2101 was reduced by the micro-sized ferrite grains. A further increase of annealing temperature to 1150 °C produced the presence of micro-sized austenite grains in the ferritic phase, due to an incomplete transformation of austenite to ferrite. They represent new sites for severe pitting attacks and therefore the corrosion resistance of LDX 2101 was the weakest. The sample annealed at 1200 °C, with few micro-sized austenite grains in the ferritic matrix, exhibited excellent corrosion resistance. Moreover, a schematic was used to illustrate the pitting corrosion of the samples annealed at different temperatures.

Keywords: lean duplex stainless steel; pitting corrosion; annealing; microstructure

1. Introduction

Duplex stainless steel (DSS) with nearly equal proportions of ferrite (α) and austenite (γ) phases, has exhibited excellent mechanical properties, corrosion resistance, and weldability, compared with the traditional austenitic and ferritic stainless steel varieties. A relatively low-cost DSS, the lean duplex stainless steels LDX 2101 with low additional amounts of Ni, are attracting more and more attention [1,2]. However, owing to its complicated structures and uneven distribution of the alloy elements in each phase, studying the corrosion resistance of LDX 2101 is complicated. The localized corrosions—including pitting, intergranular corrosion, and selective corrosion—occur at the weakest parts in the LDX 2101 matrix. It is generally accepted that pitting is one of the most detrimental and concealed forms and usually influences localized corrosion [3]. Thus, investigating the pitting corrosion resistance of LDX 2101 is necessary.

In general, the equal volume fractions of α and γ , defect-free microstructure and no deleterious phases are necessary for the good corrosion resistance of LDX 2101. However, the dual-phase balance is easily destroyed by inappropriate heat treatment. For example, DSS 2205 is susceptible to the formation

of intermetallic compounds—such as σ , χ , and Cr_2N —when it is exposed to the temperature range from 600 °C to 950 °C [4,5]. Moura et al. [6] reported that the precipitation of secondary phases, such as sigma (σ) and Cr_2N , is detrimental to the pitting resistance of DSS 2205, particularly the σ phase that is enriched with Cr and Mo [7,8]. The precipitation of this phase induces adverse changes in mechanical properties; moreover, a few volume fraction percentage points of σ phase can significantly decrease the pitting corrosion resistance of DSS 2205, due to the depletion of Cr and Mo at the grain boundaries. LDX 2101 contains lower Mo than 2205, thus the precipitation of σ is more difficult than that of DSS 2205. Zhang et al. [9] indicated that the precipitates in LDX 2101 were mainly Cr_2N , together with some Cr_{23}C_6 particles. Since the detrimental effects of Cr_2N for pitting corrosion are lower than the σ phase [10]. Studies on the corrosion resistance of LDX 2101 are mainly focused on the changes of alloy elements in α or γ phases and its phase ratio during fabrication [11,12]. Zhang et al. [13] stated that pits initially formed in the α/γ boundaries and then propagated into the ferrite phase (α) until reaching the austenite phase (γ). Westin et al. [14] addressed the effects of alloying elements and thermal cycles on the phase balance and microstructure in the high-temperature heat-affected zone of LDX 2101. Recently, Wang and Tavares [15,16] reported that the deformation-induced martensitic transformations could reduce the pitting resistance of LDX. However, studies on the dissolution and precipitation of γ phases in hot working environments and their effects on pitting corrosion in LDX 2101 are lacking.

In this study, we attempted to determine the correlation between the corrosion properties of LDX 2101 and the size or morphology of ferrite (α) and austenite (γ) by adjusting the annealing temperature. The corresponding microstructure and electrochemical characterizations were done to investigate the corrosion mechanism of LDX 2101 induced by micro-sized α and γ grains.

2. Materials and Methods

This study used a hot-rolled DSS 2101 plate with a thickness of 6 mm from Taiyuan Iron and Steel Group Co. Ltd. (Taiyuan, China) and its chemical composition is listed in Table 1. The hot-rolled plates were machined into blocks with dimensions of 14 mm \times 14 mm \times 6 mm. The specimens were solution-treated for 60 min in the desktop box-type furnace of KSL-1200X (Hefei Kejing Technology Co. Ltd., Hefei, China) at 950, 1000, 1050, 1100, 1150, and 1200 °C and then rapidly quenched in water to avoid the precipitation of Cr_2N .

Table 1. Chemical composition of the studied LDX 2101 (wt %).

Elements	C	Si	Mn	P	S	Cr	Ni	Mo	N	Fe
Content (wt. %)	0.02	0.50	5.46	0.03	0.0017	21.76	1.50	0.16	0.14	Bal.

The corrosion resistance of the specimens was evaluated using a three-electrode corrosion cell (Wuhan Corrttest Instruments Corp. Ltd., Wuhan, China) equipped with a saturated calomel electrode (SCE) reference electrode and a platinum foil counter electrode. The samples acting as working electrodes were exposed to a solution with an area of 1 cm². Before the test, the samples were ground with emery papers from 240 to 2500 grit, polished to a mirror finish and subsequently cleaned with distilled water and ethanol. Potentiodynamic polarization was conducted in 3.5 wt % NaCl aqueous solutions at room temperature, in order to test the pitting potential (E_{pit}) of the samples. E_{pit} is the potential when the corrosion current density suddenly increased. Before the measurement, the specimens were allowed to stabilize at an open circuit potential for 30 min, until the fluctuation potential was within 10 mV. The polarization curves were recorded at a scanning rate of 0.5 mV/s and the potential scanning started from less than -200 mV (relative to open circuit potential). The experiment was not terminated until the corrosion current density increased suddenly and reached 10^4 $\mu\text{A}/\text{cm}^2$. At least three specimens annealed at different temperatures were selected to repeat the electrochemical measurements in order to verify the reproducibility of the test.

The microstructure of LDX 2101 specimens were etched in the solution (0.3 g $K_2S_2O_5$ + 20 mL HCl + 80 mL H_2O) and observed under optical microscopy (OM) (Shanghai Optical Instrument Factory, Shanghai, China). Image analysis software (Image ProPlus 6.0, Media Cybernetics, Rockville, MD, USA, 2006) was used on the micrographs obtained using OM technique to quantify the vol % of α and γ phases at different temperatures. For this purpose, 10 images were taken in different zones of the samples and the final phase volume fractions were averaged. The morphology of pitting initiation sites and the contents of Cr, Mo, Ni, and Mn in the austenite and ferrite were measured using a scanning electron microscope (SEM, SCE Phillips XL30 FEG, FEI, Hillsboro, OR, USA), equipped with energy dispersive X-ray spectroscopy (EDS).

3. Results and Discussion

3.1. Microstructure Evolution during Annealing Treatment

The microstructure of the samples annealed at different temperatures for 60 min are shown in Figure 1a–f, which were observed using OM. Typical duplex structures were observed in all specimens. Moreover, the γ phase (the bright phase) was uniformly distributed in the ferritic matrix (the relatively dark phase). The microstructure of the samples was elongated along the rolling direction and few precipitates were found in the annealed specimens. Furthermore, the γ phases gradually dissolved as the annealing temperature increased, suggesting that a typical diffusion-controlled solid-state phase transformation occurred: $\gamma \rightarrow \alpha$ [17]. This result was confirmed by quantitative metallography in depth, as shown in Figure 2. Phase volume fraction strongly depends on the annealing temperature, showing a linear trend for the γ and α phases [18].

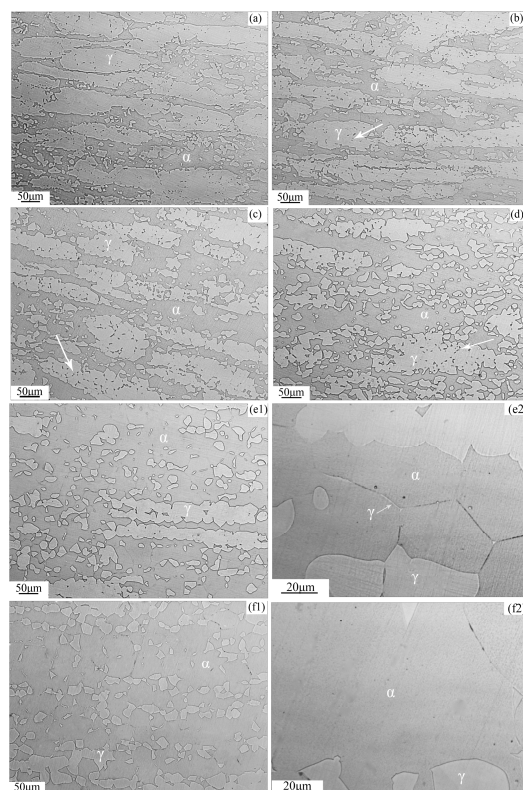


Figure 1. Optical microstructure of the LDX 2101 samples after annealing for 60 min at different temperatures: (a) 950 °C, (b) 1000 °C, (c) 1050 °C, (d) 1100 °C, (e) 1150 °C, (f) 1200 °C: (e2,f2) are the local amplification areas of the (e1,f1) respectively, the arrows in (b–d) and (e2) indicate the micro-sized α grains transformed from γ phases in austenite domains and the micro-sized γ grains that are not completely transformed into α phases in ferrite matrix, respectively.

As the annealing temperature increased from 950 °C to 1050 °C, the elongated γ islands with typical ribbon-like morphology were embedded in the gray etched α matrix and the distribution of the two phases became increasingly homogeneous. Additionally, there were many micro-sized ferrite grains that were newly produced from γ due to the $\gamma \rightarrow \alpha$ transformation in austenite domains as shown in Figure 1b,c, especially at 1050 °C. When the annealing temperature increased further, as shown in Figure 1d–f, the micro-sized ferrite grains in austenite domains decreased and the band-shaped α grains gradually widened [19,20]. Moreover, many small-sized γ phases appeared in the ferrite regions that were attributed to the not complete transformation of γ phase into α phase, with the increase of annealing temperature. In particular, as shown in Figure 1(e2), the γ phases in the sample annealed at 1150 °C became slender and it is similar to a line. We defined it as micro-sized γ phases. However, the micro-sized γ shown in Figure 1(e2) almost disappeared when the annealing temperature was 1200 °C. The specific observation is shown in the Figure 1(f2).

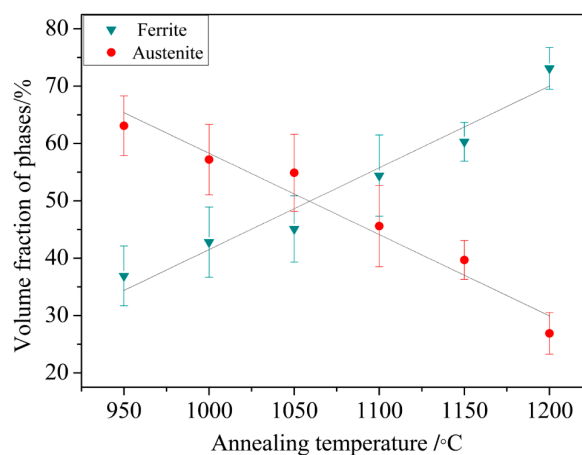


Figure 2. Volume fraction of ferrite and austenite phase annealed at different temperatures.

3.2. Influence of Annealing Temperature on Electrochemical Corrosion

Potentiodynamic polarization was used to characterize the pitting resistance of the annealed LDX 2101. The typical polarization curves in 3.5 wt % sodium chloride solution in Figure 3 illustrate one of the recorded measurements for each annealing temperature.

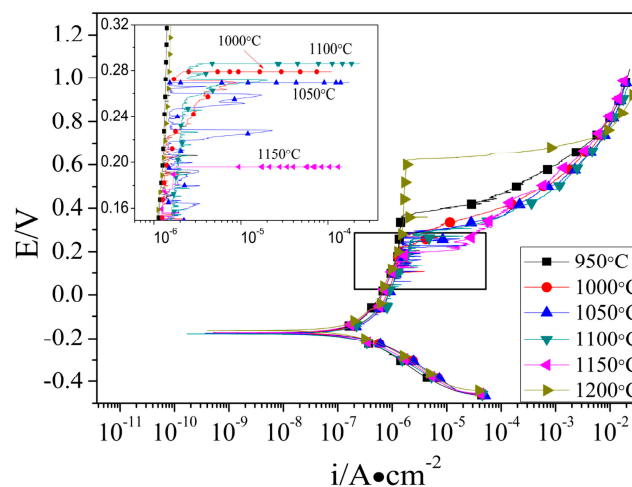


Figure 3. Potentiodynamic anodic polarization curves of the LDX 2101 with different annealing temperatures in 3.5 wt % sodium chloride solution.

The E_{pit} of samples annealed at 1200 °C were the highest, followed by those at 950 °C. However, the E_{pit} of samples annealed from 1000 °C to 1100 °C were similar to each other and the samples annealed at 1150 °C had the lowest E_{pit} . Many current peaks, associated with the events of metastable pitting were observed before the appearance of stable pitting in all tested specimens [21]. As the temperature increased from 950 °C to 1050 °C, the E_{pit} gradually decreased, indicating that the corrosion resistance of LDX 2101 was deteriorated by the increased ferrite. This result is uniform with the phenomena found by Lai et al. [22]. When the annealing temperature reached 1100 °C, the E_{pit} of the sample became slightly higher than the samples that were annealed at 1000 °C and 1050 °C. Thus, the results of the polarization curves indicate that phase volume fraction is not the only factor that affects the pitting corrosion resistance of LDX 2101. There is also an effect of the microstructure of the studied alloy as will be shown in the next section.

3.3. Pitting Corrosion Evolution as a Function of Annealing Temperature

Figure 4 shows the pit morphologies after the potentiodynamic polarization tests of LDX 2101. Pit morphologies of the specimens annealed at 950, 1000, 1050, and 1100 °C in Figure 4a–d showed that pitting was initiated at the α/γ boundaries or within the ferrite domains and then propagated into the ferrite. However, at 1000, 1050, and 1100 °C, the α/γ boundaries formed by austenite with the micro-sized ferrite grains in austenite zones were preferentially attacked by pits and even some micro-sized ferrite phases were completely corroded. Moreover, this phenomenon was highly significant at 1050 °C thereby lowering the pitting corrosion resistance. Once the annealing temperature achieves 1150 °C, the pit locations appear to have changed and it might occur in the so-called grain boundaries of ferrite as displayed in Figure 4e. To further confirm this phenomenon, the grain boundaries of ferrite were magnified and characterized by SEM. As shown in Figure 5, the γ phase still exists in the α grain boundaries and is relatively small at the microscale level. This result could be attributed to the diffusion-controlled solid-state phase transformation of γ into α , corresponding to the OM observation in the Figure 1(e2). The presence of micro-sized γ grains in the ferrite domains maintains the α/γ boundaries susceptible of pitting corrosion. Moreover, the two α/γ boundaries are close as shown in Figure 5b and therefore the micro-sized γ can be removed easily when corrosion occurred in the α/γ boundaries. The micro-sized γ phase gradually dissolved and disappeared with the annealing temperature increase to 1200 °C thereby improving the corrosion resistance of LDX 2101. The pitting occurred within the ferrite grains after annealing at 1200 °C in Figure 4f demonstrated the definitive disappearance of micro-sized γ phase in the α grain boundaries, as a preferential site for localized corrosion attack. Therefore, for the annealed samples at relatively low temperatures, the corrosion was preferentially initiated at the α/γ boundaries or within ferrite domains: micro-sized ferrite grains play an important role on the corrosion resistance at these temperatures. However, the micro-sized γ influences the corrosion resistance of the sample annealed at relatively high temperatures.

The schematic of Figure 6 shows the effects of γ dissolution ($\gamma \rightarrow \alpha$) on pitting initiation and propagation in LDX 2101 as a function of the annealing temperature. As shown in Figure 6a, pits mainly nucleate in the α/γ phase boundaries or within ferrite domains and propagate into α at a relatively low temperature (950 °C). As γ continually dissolves with the temperature increase from 1000 °C to 1100 °C, the pitting is mainly due to the selective corrosion of the newly produced and micro-sized ferrite from the α/γ phase boundaries in austenite domains, which is shown in Figure 6b. When austenite remains in form of micro-sized γ , shown in Figure 1(e2), due to incomplete transformation γ into α , the mechanism of pitting corrosion is the selective dissolution of micro-sized γ , as shown in Figure 6c. Then γ grains continue to dissolve with the annealing temperature increase until the micro-sized γ completely dissolved to disappear, as shown in Figure 1f, and consequently the pitting only occurs within the ferrite regions, as shown in Figure 6d.

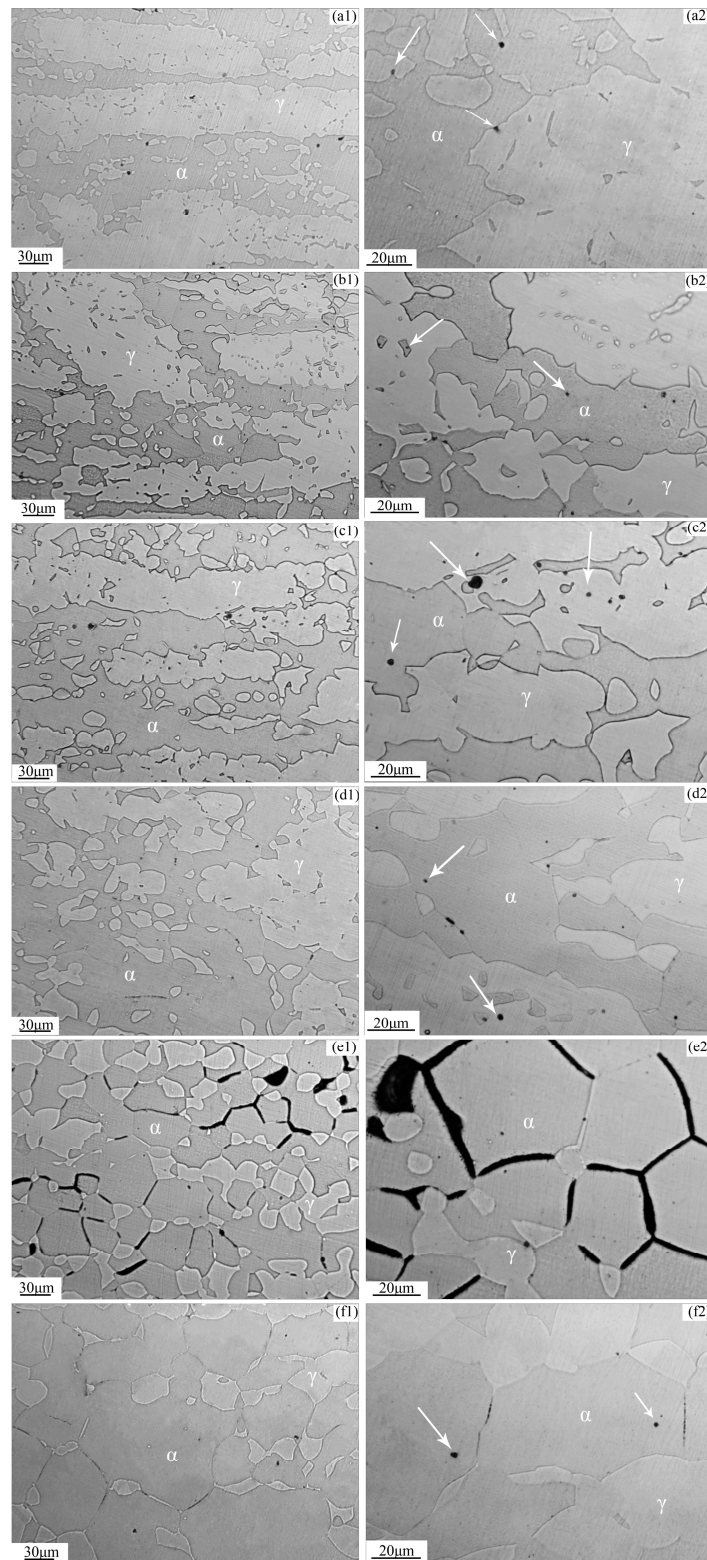


Figure 4. Micrographs of pits surface of the LDX 2101 annealed at different temperatures after the potentiodynamic anodic polarization tests: (a) 950 °C, (b) 1000 °C, (c) 1050 °C, (d) 1100 °C, (e) 1150 °C, (f) 1200 °C, the arrows in (a2–d2) and (f2) indicate the pits.

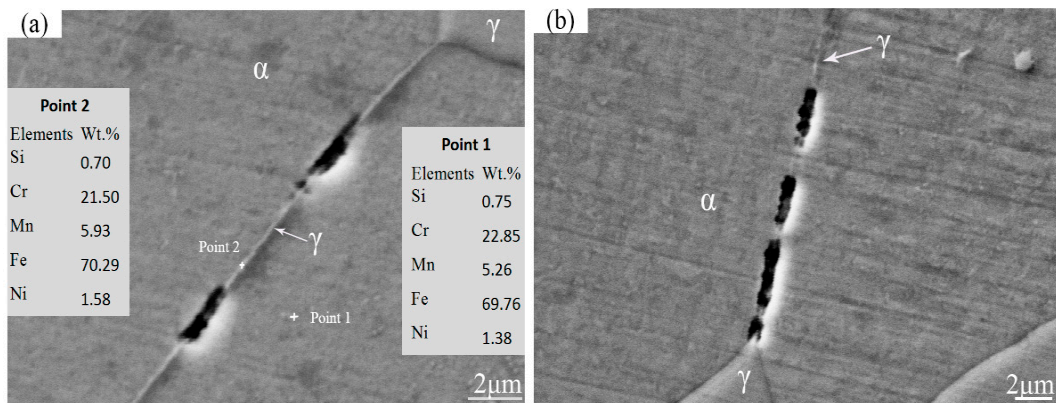


Figure 5. The SEM of the LDX 2101 annealed at 1150 °C after the potentiodynamic anodic polarization test.

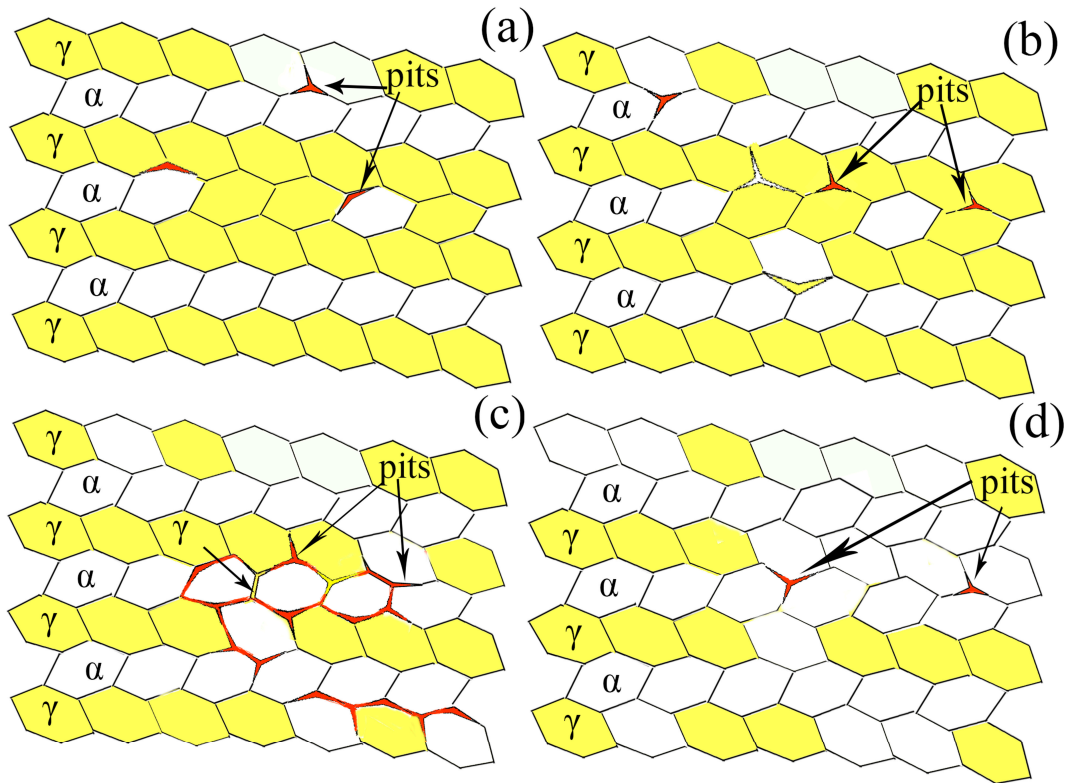


Figure 6. Schematic of the pitting initiation and propagation of the LDX 2101 at different temperatures: (a) 950 °C, (b) 1000, 1050, and 1100 °C, (c) 1150 °C, (d) 1200 °C.

4. Conclusions

The microstructural characteristics of LDX 2101 were affected by annealing treatment at different temperatures, which unavoidably exerted influence on the tendency of a stainless steel to pitting corrosion. Results indicated that, as temperature increased from 950 °C to 1100 °C, pitting was initiated preferentially at the α/γ boundaries or within the ferrite domains and then propagated into α phase. Moreover, as the annealing temperature ranged from 1000 °C to 1100 °C, the micro-sized ferrite grains were newly produced from γ phases due to the $\gamma \rightarrow \alpha$ transformation in austenite domains, especially at 1050 °C. These micro-sized ferrite grains represent new sites for pitting corrosion attack at these intermediate temperatures. Therefore, the pitting corrosion resistance gradually decreased with

temperature increase from 950 °C to 1100 °C. When temperature increased to 1150 °C, the micro-sized γ grains present in ferrite domains were new sites of severe pitting attacks, which significantly reduced the corrosion resistance of LDX 2101. Finally, the corrosion resistance of samples annealed at 1200 °C, showing only a negligible presence of micro-sized γ grains in the α matrix, was excellent.

Acknowledgments: This work was supported by the National Natural Science Foundation of China (Grant No. 51371123), the Research Fund for the Doctoral Program of Higher Education of China (No. 2013140211003), Shanxi Natural Science Foundation Project (No. 2014011002-1, No. 201601D202034) and Innovation Project for Graduate Education of Shanxi province (No. 2016JD20).

Author Contributions: Peide Han, Jian Wang, and Yuping Li helped to conceive and design the experiments; Yadi Hu and Yan He performed the experiments; Xinglong Liu and Yong Zhang helped to fulfill the experiments; Yadi Hu and Peide Han analyzed the data; Hu Yadi wrote the paper.

Conflicts of Interest: The authors declare no conflict of interest. The founding sponsors had no role in the design of the study.

References

1. Charles, J. Duplex stainless steels—A review after DSS '07 held in Grado. *Steel Res. Int.* **2008**, *105*, 455–465. [[CrossRef](#)]
2. Rosso, M.; Peter, I. About heat treatment and properties of duplex stainless steels. *J. Achiev. Mater. Manuf. Eng.* **2013**, *59*, 26–36.
3. Toor, I.-H.; Hyun, P.J. Development of high Mn-N duplex stainless steel for automobile structural components. *Corros. Sci.* **2008**, *50*, 404–410. [[CrossRef](#)]
4. Ezuber, H.; El-Houd, M.A. Effects of sigma phase precipitation on seawater pitting of duplex stainless steel. *Desalination* **2007**, *207*, 268–275. [[CrossRef](#)]
5. Ravindranath, K.; Malhotra, S.N. The influence of aging on the intergranular corrosion of 22 chromium-5 nickel duplex stainless steel. *Corros. Sci.* **1995**, *37*, 121–132. [[CrossRef](#)]
6. Moura, V.S.; Lima, L.D. Influence of microstructure on the corrosion resistance of the duplex stainless steel UNS S31803. *Mater. Charact.* **2008**, *59*, 1127–1132. [[CrossRef](#)]
7. Pohl, M.; Storz, O. Sigma phase in duplex-stainless steels. *Z. Metallkd.* **2004**, *95*, 631–638. [[CrossRef](#)]
8. Sathirachinda, N.; Pettersson, R. Depletion effects at phase boundaries in 2205 duplex stainless steel characterized with SKPFM and TEM/EDS. *Corros. Sci.* **2009**, *51*, 1850–1860. [[CrossRef](#)]
9. Zhang, W.; Jiang, L.Z. Study of precipitation in 2101 duplex stainless steel. *Mater. Sci. Technol.* **2010**, *26*, 515–521. [[CrossRef](#)]
10. Zhang, L.; Jiang, Y. Effect of aging on the corrosion resistance of 2101 lean duplex stainless steel. *Mater. Charact.* **2009**, *60*, 1522–1528. [[CrossRef](#)]
11. Cervo, R.; Ferro, P. Annealing temperature effects on super duplex stainless steel UNS S32750 welded joints. II: Pitting corrosion resistance evaluation. *J. Mater. Sci.* **2010**, *45*, 4378–4389. [[CrossRef](#)]
12. Deng, B.; Jiang, Y.M. Effect of annealing treatment on microstructure evolution and the associated corrosion behaviour of a super-duplex stainless steel. *J. Alloys Compd.* **2010**, *493*, 461–464. [[CrossRef](#)]
13. Zhang, L.; Zhang, W. Influence of annealing treatment on the corrosion resistance of lean duplex stainless steel 2101. *Electrochim. Acta* **2009**, *54*, 5387–5392. [[CrossRef](#)]
14. Westin, E.M.; Brolund, B. Weldability aspects of a newly developed duplex stainless steel LDX 2101. *Steel Res. Int.* **2008**, *79*, 473–481. [[CrossRef](#)]
15. Wang, K.Y.; Lo, K.H. The influences of martensitic transformations on cavitation-erosion damage initiation and pitting resistance of a lean austenitic stainless steel. *Mater. Res.* **2016**, *19*, 1366–1371. [[CrossRef](#)]
16. Tavares, S.S.M.; Pardal, J.M. Martensitic transformation induced by cold deformation of lean duplex stainless steel UNS S32304. *Mater. Res.* **2014**, *17*, 381–385. [[CrossRef](#)]
17. Ha, H.Y.; Jang, M.H. Interpretation of the relation between ferrite fraction and pitting corrosion resistance of commercial 2205 duplex stainless steel. *Corros. Sci.* **2014**, *89*, 154–162. [[CrossRef](#)]
18. Lacerda, J.C.D.; Cândido, L.C. Effect of volume fraction of phases and precipitates on the mechanical behavior of UNS S31803 duplex stainless steel. *Int. J. Fatigue* **2015**, *74*, 81–87. [[CrossRef](#)]
19. Nie, H.; Xiong, J. Effects of multi-scale microstructure on pitting corrosion and mechanical properties of high-Mn-N low-Ni superduplex stainless steel. *Rare Met. Mater. Eng.* **2012**, *41*, 575–580.

20. Tan, H.; Jiang, Y. Effect of annealing temperature on the pitting corrosion resistance of super duplex stainless steel UNS S32750. *Mater. Charact.* **2009**, *60*, 1049–1054. [[CrossRef](#)]
21. Moayed, M.H.; Newman, R.C. Evolution of current transients and morphology of metastable and stable pitting on stainless steel near the critical pitting temperature. *Corros. Sci.* **2006**, *48*, 1004–1018. [[CrossRef](#)]
22. Lai, J.K.L.; Wong, K.W. Effect of solution treatment on the transformation behavior of cold-rolled duplex stainless steels. *Mater. Sci. Eng. A* **1995**, *203*, 356–364. [[CrossRef](#)]



© 2017 by the authors. Licensee MDPI, Basel, Switzerland. This article is an open access article distributed under the terms and conditions of the Creative Commons Attribution (CC BY) license (<http://creativecommons.org/licenses/by/4.0/>).